TASK QUARTERLY 15 No 2, 135–155

TWO-DIMENSIONAL MODEL OF FLUID FLOW AND DISTRIBUTION OF NUTRIENT CONCENTRATION IN A MICROFLUIDIC DEVICE

PAWEŁ WRONISZEWSKI

Institute of Fluid-Flow Machinery, Polish Academy of Sciences,
Fiszera 14, 80-952 Gdansk, Poland
pwronisz@gmail.com

(Received 17 December 2010; revised manuscript received 25 February 2011)

Abstract: During the past few years, the process of miniaturisation in the field of biochemical laboratory equipment led to the introduction of the so-called "lab-on-a-chip" microdevices, which combine separate functional units into a complex, multifunctional apparatus. Fluid dynamics plays an essential role in the development of such equipment, since frequently the major part of chemical analysis is based on soluble analytes. In this work, we consider a device for the analysis of cell growth under different conditions.

In this device, dozens of cell spots absorb the nutrient (analyte) from the liquid medium. The concentration of the analyte must be strictly controlled to maintain a specific microenvironment. A two-dimensional model for the flow field and the distribution of concentration of the analyte is developed taking into account the geometrical shape of the spot with a simplified absorption model. The dependence of the results on the controlling parameters is investigated in order to determine the influence of the presence of the cell spot on the distribution of the analyte.

Keywords: microfluidic device, lab-on-a-chip, advection-diffusion equation, Taylor dispersion

1. Introduction

In the device considered in this work, we investigate the growth of stem cells consuming a nutrient [1, 2]. The considered domain is a shallow channel, in which the fluid moves slowly transporting the analyte (nutrient) to the spots of cells. Such an interrogation chamber can be connected to other microfluidic elements, such as micropumps or mixers, in order to create a complete microanalysis system [3, 4]. Each cell spot distributed along the channel consumes the nutrient from the liquid medium, resulting in a depletion area. The rate of smoothing of the depleted wake is of major interest, as it affects the microenvironment of the cells downstream.

This work does not constitute the first attempt to develop a model for the flow in the considered type of microdevice. A model for the concentration distribution in a simplified channel with parallel horizontal walls has already been proposed [5]. The consumption of the analyte by the cells was described using Michaelis-Menten kinetics, which is a fairly complex and realistic description, taking into account the dependence of the intensity of consumption on the concentration of the nutrient.

In the present work, the stationary flow around a single cell spot is studied, with full consideration of the geometrical shape of the spot itself. For simplicity, the cell consumption is represented by a prescribed consumption flux.

1.1. Governing equations

The distribution of concentration $c = c(x,y,z)$ for incompressible flow is governed by the advection-diffusion equation of the following form:

$$\frac{\partial c}{\partial t} + \boldsymbol{u} \cdot \nabla c = D \nabla^2 c \tag{1}$$

The equation describes a conservation law for the total flux of the nutrient, which consists of two terms – a convective term, due to the fluid flow ($\boldsymbol{u} = \boldsymbol{u}(x,y,z)$ – velocity vector), and a diffusive term – due to the molecular diffusion in the fluid (D – diffusion coefficient). In the steady case considered in this paper, the local time derivative $\frac{\partial c}{\partial t}$ vanishes. To solve the problem, the velocity distribution is required, This distribution is governed by the Navier-Stokes equation:

$$(\boldsymbol{u} \cdot \nabla)\boldsymbol{u} + \frac{1}{\rho}\nabla p - \nu \nabla^2 \boldsymbol{u} = 0 \tag{2}$$

where $p = p(x,y,z)$ is the pressure, and the continuity law:

$$\nabla \boldsymbol{u} = 0 \tag{3}$$

These two problems are uncoupled, therefore first we calculate the velocity field, subsequently inserting the results into the advection-diffusion equation.

Solving problems in their three-dimensional form is time-consuming and thus not suitable for working with a large set of parameters. Therefore, we developed a two-dimensional model by averaging the equations over the vertical direction. A distribution of the averaged concentration was obtained, which we believe to contain all the crucial information about the problem. During the averaging of the advection-diffusion equation, additional terms of lower order appear. The treatment of these terms, described in the following sections, constitutes the focal point of this work.

1.2. Taylor dispersion

The effect of Taylor dispersion is encountered in shear flows with diffusion, where an increase in the effective diffusivity can be observed. It was first described by Taylor in his seminal work on dispersion in pipe flow [6]. If a spot of a concentrated analyte in a channel is considered, high gradients of concentration in the longitudinal direction are observed on the borders of the spot. In a constant

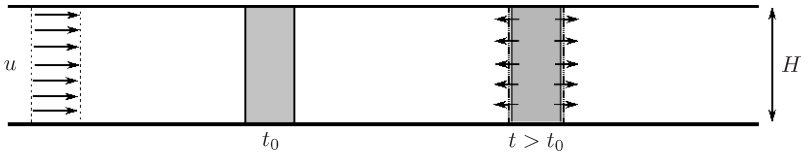

Figure 1. Transport of the spot of concentrated analyte in a constant velocity field; the short vectors on the borders of the spot represent the flux due to diffusion

velocity field, the spot is transported downstream, with diffusion acting solely in the longitudinal direction (Figure 1).

In the case of shear flow, *e.g.* of a parabolic shape, Equation (26), the spot is stretched and the diffusion acts also in the transverse direction, relatively quickly smoothing out the gradient of concentration, due to a different spatial scale $H/L = \epsilon \ll 1$ and a larger surface on which the gradient is distributed (Figure 2).

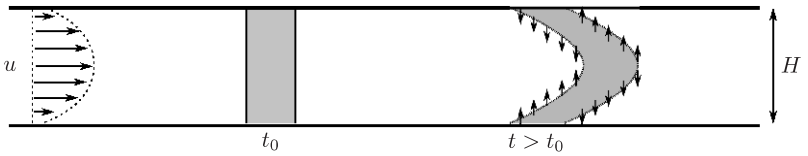

Figure 2. Transport of the spot of concentrated analyte in a parabolic velocity field

The described effect was first observed for unsteady cases and proved to be of crucial importance. Still, if the stationary advection-diffusion equation is averaged over the transverse direction of the flow, there appears a correction to the diffusion coefficient, which is a function of the average velocity. The Study Group [5] obtained the correction for the case of a channel with two parallel plates. In this paper, a similar procedure is undertaken for the case of a channel of variable height, taking into account the presence of the spot. A correction to the diffusion coefficient with both components of velocity is obtained.

1.3. Scaling of the problem

We derive a set of equations describing the flow in a thin domain, whose height varies slowly due to the presence of the cell spot at the bottom of the channel (Figure 3). The shape of the bottom of the channel is described by a given function $h(x,y)$.

An important insight into the flow in the considered domain is gained after a suitable transformation of the governing equations (3)–(2) into dimensionless form. This procedure helps us distinguish the most important terms in the equations. The key parameter that determines the scale for the spatial variations in the flow is the diameter of the cell spot R_s. It is assumed to be significantly larger than the height H of the domain, therefore the aspect ratio ϵ is:

$$\epsilon = \frac{H}{R_s} \ll 1 \tag{4}$$

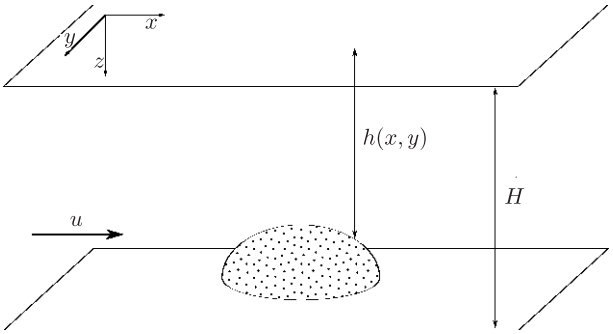

Figure 3. Domain

These parameters, together with the characteristic flow velocity u_0, determine the scale for the components of the velocity vector $\boldsymbol{u} = [u,v,w]$, $u = u(x,y,z)$, $v = v(x,y,z)$, $w = w(x,y,z)$ and the pressure $p(x,y,z)$:

$$(x_*, y_*) = \frac{(x,y)}{R_s}, \qquad z_* = \frac{z}{H}, \qquad h_* = \frac{h}{H} \tag{5}$$

$$(u_*, v_*) = \frac{(u,v)}{u_0}, \qquad w_* = \frac{w}{\epsilon u_0}, \qquad p_* = \frac{pH^2}{\rho\nu R_s u_0} \tag{6}$$

where "$*$" denotes dimensionless variables. In order to determine a suitable value for the constant that would provide the dimensional scaling of velocity in the z direction, we balanced all the terms in the continuity equation (3), assuming $\frac{u_0}{R_s} \sim \frac{w_0}{H}$ and $w_0 \sim \epsilon u_0$. For the pressure, we balanced the leading terms of the N-S equation (2), in the sense of $\nu\frac{u_0}{H^2} \sim \frac{1}{\rho}\frac{p_0}{R_s}$.

Owing to such scaling, the dimensionless form of the continuity equation has a simple form:

$$\frac{\partial u_*}{\partial x_*} + \frac{\partial v_*}{\partial y_*} + \frac{\partial w_*}{\partial z_*} = 0 \tag{7}$$

Hereinafter we omit "$*$" for convenience. The dimensionless Navier-Stokes equation for each component has the form:

$$\epsilon\mathrm{Re}\left(u\frac{\partial u}{\partial x} + v\frac{\partial u}{\partial y} + w\frac{\partial u}{\partial z}\right) + \frac{\partial p}{\partial x} - \epsilon^2\left(\frac{\partial^2 u}{\partial x^2} + \frac{\partial^2 u}{\partial y^2}\right) - \frac{\partial^2 u}{\partial z^2} = 0 \tag{8}$$

$$\epsilon\mathrm{Re}\left(u\frac{\partial v}{\partial x} + v\frac{\partial v}{\partial y} + w\frac{\partial v}{\partial z}\right) + \frac{\partial p}{\partial y} - \epsilon^2\left(\frac{\partial^2 v}{\partial x^2} + \frac{\partial^2 v}{\partial y^2}\right) - \frac{\partial^2 v}{\partial z^2} = 0 \tag{9}$$

$$\epsilon^3\mathrm{Re}\left(u\frac{\partial w}{\partial x} + v\frac{\partial w}{\partial y} + w\frac{\partial w}{\partial z}\right) + \frac{\partial p}{\partial z} - \epsilon^4\left(\frac{\partial^2 w}{\partial x^2} + \frac{\partial^2 w}{\partial y^2}\right) - \epsilon^2\frac{\partial^2 w}{\partial z^2} = 0 \tag{10}$$

where

$$\mathrm{Re} = \frac{u_0 H}{\nu} \tag{11}$$

is the Reynolds number. According to the estimates provided in [5], Table 1 reports typical values of the parameters for the considered type of microdevice.

Table 1. Typical values of relevant dimensional parameters

Symbol	Parameter	Size	Unit
H	Height of the channel	$10^{-4}-10^{-5}$	m
R_s	Diameter of the cell spot	10^{-3}	m
H_s	Height of the cell spot	$2-5\cdot10^{-6}$	m
u_0	Mean velocity	$\sim10^{-5}$	m/s
ν	Kinematic viscosity of the fluid	$0.725\cdot10^{-6}$	m^2/s
c_0	Input bulk concentration	$10^{-6}-10^{-4}$	mol/m^3
D	Diffusion coefficient	$10^{-11}-10^{-10}$	m^2/s
L_c	Distance between two spots	10^{-2}	m

According to this, the Reynolds number is expected to be equal to 10^{-3}. Obviously, $\epsilon = \frac{H}{R_s} \sim 10^{-1}-10^{-2}$ satisfies the previous assumptions (4). The Navier-Stokes equations can be approximated to the leading order as:

$$\frac{\partial p}{\partial x} = \frac{\partial^2 u}{\partial z^2} \tag{12}$$

$$\frac{\partial p}{\partial y} = \frac{\partial^2 v}{\partial z^2} \tag{13}$$

$$\frac{\partial p}{\partial z} = 0 \tag{14}$$

As can be seen from Table 1, the height of the spot can be in the range of 0.02 to 0.5 of the height of the channel. This means that, in general, the influence of the shape of the spot on the velocity field should be taken into account.

The flow in the microdevice is pressure-driven and is characterised by low values of the Reynolds number, therefore it is expected to be laminar. The analyte can only move in the direction transverse to the flow by means of diffusion. By scaling the concentration as $c_* = \frac{c}{c_0}$ and using the earlier assumptions for the remaining variables (5)–(6), we obtain the dimensionless advection-diffusion equation in the form:

$$\left(u\frac{\partial}{\partial x} + v\frac{\partial}{\partial y} + w\frac{\partial}{\partial z}\right)c = \frac{1}{\mathrm{Pe}}\left(\frac{\partial^2}{\partial x^2} + \frac{\partial^2}{\partial y^2}\right)c + \frac{1}{\epsilon^2\mathrm{Pe}}\frac{\partial^2}{\partial z^2}c \tag{15}$$

where

$$\mathrm{Pe} = \frac{R_s u_0}{D} \sim 10^2 - 10^3 \tag{16}$$

is the Peclet number, which is the measure of the ratio of the strength of advection with respect to the diffusion in the considered problem.

2. Fluid flow around a single cell spot

2.1. Boundary conditions

To complete the formulation of the problem, the boundary conditions (BCs) need to be specified. The inlet and outlet can be represented by $x \in \{0, L\}$, while the vertical walls of the computational domain are given by $y \in \{0, W\}$. Owing to the presence of the cell spot, only the top of the channel is flat ($z = 0$), while

the bottom profile is described by $z = h = h(x,y) \in (0,1]$ (Figure 3), and can be defined using the function:

$$F(x,y,z) = h(x,y) - z \tag{17}$$

with $F(x,y,z) = 0$.

One can define the vector normal to the bottom of the channel as:

$$\boldsymbol{n}|_{z=h} = \frac{\nabla F}{|\nabla F|} = \frac{1}{\sqrt{\left(\frac{\partial h}{\partial x}\right)^2 + \left(\frac{\partial h}{\partial x}\right)^2 + 1}} \left[\frac{\partial h}{\partial x}, \frac{\partial h}{\partial y}, -1\right] \tag{18}$$

For the pressure, the constant values at the inlet and the outlet and a no-flux BCs at the side walls are assumed:

$$p|_{x=0} = p_{in}, \qquad p|_{x=L} = p_{out} \tag{19}$$

$$\left.\frac{\partial p}{\partial y}\right|_{y=\{0,W)} = 0, \qquad \left.\frac{\partial p}{\partial z}\right|_{z=0} = 0, \qquad \boldsymbol{n} \cdot \nabla p|_{z=h} = 0 \tag{20}$$

The last condition can be rewritten using the vector $\boldsymbol{n}$, Equation (18) as:

$$\left.\frac{\partial p}{\partial z}\right|_{z=h} = \epsilon^2 \left(\frac{\partial h}{\partial x}\frac{\partial p}{\partial x} + \frac{\partial h}{\partial y}\frac{\partial p}{\partial y}\right)\Bigg|_{z=h} \tag{21}$$

For the velocity, the no-slip condition on the horizontal walls of the channel reads:

$$\boldsymbol{u}|_{z=\{0,h\}} = 0 \tag{22}$$

The value of the velocity is expected to remain constant in the areas of the inlet, outlet and the vertical side walls of the computational domain:

$$\left.\frac{\partial \boldsymbol{u}}{\partial x}\right|_{x=\{0,L\}} = \left.\frac{\partial \boldsymbol{u}}{\partial y}\right|_{y=\{0,W\}} = 0 \tag{23}$$

2.2. Calculation of the pressure and velocity fields

From the third dimensionless Navier-Stokes equation (14) it is clear that the pressure does not depend on the z coordinate, therefore $p = p(x,y)$. Now, using the no-slip boundary conditions (22) it is easy to solve the two remaining N-S equations (12)–(13) for u and v, obtaining:

$$[u,v] = -\frac{1}{2} z(h-z) \left[\frac{\partial p}{\partial x}, \frac{\partial p}{\partial y}\right] \tag{24}$$

The above equations show that the vertical components of the velocity are proportional to the gradient of the pressure and that the velocity profile is parabolic in the z direction. This flow is known in the literature as Hele-Shaw

flow. The velocity field can be calculated as soon as the pressure distribution is known. The vertically-averaged velocity is defined as:

$$[\bar{u},\bar{v}] = \frac{1}{h}\int_0^h [u,v]\,dz = -\frac{h^2}{12}\left[\frac{\partial p}{\partial x},\frac{\partial p}{\partial y}\right] \tag{25}$$

Owing to the above equation, we can write:

$$[u,v] = [\bar{u},\bar{v}]\,\frac{6}{h^2}z(h-z) \tag{26}$$

By using the continuity equation (7) along with the above relations, the z component of the velocity can be calculated as:

$$w = -6\left(\frac{z^2}{2h}-\frac{z^3}{3h^2}\right)\left(\frac{\partial \bar{u}}{\partial x}+\frac{\partial \bar{v}}{\partial y}\right)+6\left(\frac{z^2}{2h^2}-\frac{2z^3}{3h^3}\right)\left(\bar{u}\frac{\partial h}{\partial x}+\bar{v}\frac{\partial h}{\partial y}\right) \tag{27}$$

By using the derivatives of the obtained solutions of the N-S equation (24) and the no-slip boundary conditions (22), the continuity equation (7) can be integrated along the z direction to obtain:

$$\frac{\partial}{\partial x}\left(h^3\frac{\partial p}{\partial x}\right)+\frac{\partial}{\partial y}\left(h^3\frac{\partial p}{\partial y}\right)=0 \tag{28}$$

The above equation can be solved numerically, together with the given boundary conditions (19)–(20). The values p_{in} and p_{out} are chosen so that the average velocity calculated with Equation (25) using a finite difference is equal to u_0.

The above equation is similar to the equation of the two-dimensional stationary heat transfer in a non-homogeneous medium without sources [7]. It was solved using the finite volume method [7, 8] on a regular 2D mesh of control volumes (CVs) by integrating Equation (28) over each control volume. To calculate the fluxes between the CVs, we assumed a linear distribution of pressure between the nodes and a constant distribution of height over the boundaries of the CVs. As a result, a single algebraic equation was obtained for each node.

To solve this set of algebraic equations, the *alternating-direction implicit* (ADI or *line-by-line*) method was used [8]. In this method, having chosen initial values for all the grid points, the values for a single grid line are treated as unknowns and all values in the neighbouring nodes – as given. A resulting tridiagonal matrix must be solved using *e.g.* the Gaussian elimination algorithm. The procedure is repeated for each line in both directions in order to complete one iteration of the method. Iterations are repeated until a prescribed convergence condition is satisfied.

When the pressure field is known, the averaged velocity field (25) can be calculated numerically with finite differences. The velocity field is given at the boundaries of the control volumes. A staggered grid of this type is particularly suitable for the given uncoupled problem and can be easily incorporated into the advection-diffusion equation.

3. Transport of the analyte

3.1. Advection-diffusion equation

Owing to the continuity equation (7), the advection-diffusion equation (1) can be written in the form:

$$\frac{\partial}{\partial x}(uc)+\frac{\partial}{\partial y}(vc)+\frac{\partial}{\partial z}(wc)=\frac{1}{\mathrm{Pe}}\left(\frac{\partial^2}{\partial x^2}+\frac{\partial^2}{\partial y^2}\right)c+\frac{1}{\epsilon^2\mathrm{Pe}}\frac{\partial^2}{\partial z^2}c \tag{29}$$

To formulate the problem, suitable boundary conditions for the concentration must be imposed. A given value of concentration c_0 at the inlet is assumed, which in the dimensionless form translates into $c|_{x=0}=1$, and a no-flux condition at the walls is also assumed. In particular, for the upper boundary we have:

$$\left.\frac{\partial c}{\partial z}\right|_{z=0}=0 \tag{30}$$

As for the lower boundary, we assume the flux $\frac{\delta}{D}q(x,y)$ generated by the consumption of the analyte by the cells. The dimensionless function $q(x,y)$ describes the spatial distribution of the intensity of consumption, while δ is the dimensional flux magnitude. The vector $\boldsymbol{n}$ is normal to the lower boundary and is directed towards the fluid. The BC can be written as:

$$\boldsymbol{n}\cdot\nabla c|_{z=h}=\boldsymbol{n}\cdot\frac{c_0}{R_s}\left[\frac{\partial c}{\partial x},\frac{\partial c}{\partial y},\frac{1}{\epsilon}\frac{\partial c}{\partial z}\right]\Bigg|_{z=h}=\frac{\delta}{D}q \tag{31}$$

The flux into the surface of the cell significantly depletes the fluid from the analyte. Therefore, the uptake on the length R_s is expected to be similar to the flux, *i.e.* $R_s\delta\sim u_0Hc_0$. Therefore, $\frac{R_s\delta}{c_0D}=\epsilon\mathrm{Pe}$. Using the vector normal to the bottom of the channel (18), and expanding it into a Taylor series $\sqrt{1+\epsilon x}=\sqrt{1}+\frac{\epsilon}{2}x+\ldots$, we can write:

$$\left.\frac{\partial c}{\partial z}\right|_{z=h}=-\epsilon^2\mathrm{Pe}q+\epsilon^2\left(\frac{\partial h}{\partial x}\frac{\partial c}{\partial x}+\frac{\partial h}{\partial y}\frac{\partial c}{\partial y}\right)\Bigg|_{z=h}-O\left(\epsilon^4\mathrm{Pe}\right) \tag{32}$$

We will subsequently neglect terms of order $\epsilon^4\mathrm{Pe}$.

3.2. Averaged advection-diffusion equation

To calculate the average of the advection-diffusion equations (15) and (29), a suitable averaging operator is defined as:

$$\langle\square\rangle=\bar{\square}=\frac{1}{h}\int_0^h\square\,dz \tag{33}$$

Using one of the basic rules of calculus for the function $G(x,y)=\int_0^{h(x,y)}g(x,y,z)\,dz$, the derivative can be obtained:

$$\frac{\partial}{\partial x}G(x,y)=\int_0^{h(x,y)}\frac{\partial}{\partial x}g(x,y,z)\,dz+g(x,y,z)|_{z=b(x,y)}\frac{\partial h}{\partial x} \tag{34}$$

The second derivative can be calculated similarly, yielding:

$$\int_0^h g_x\,dz=(h\bar{g})_x-g|_h h_x \tag{35}$$

$$\int_0^h g_{xx}\,dz = (h\bar{g})_{xx} - \left(2g_x h_x + g h_{xx} + g_z h_x^2\right)\big|_h \tag{36}$$

The subscripts x, y and z denote derivatives with respect to corresponding coordinates.

Due to the above relations and suitable boundary conditions (22), the averaged continuity equation has a simple form:

$$(h\bar{u})_x + (h\bar{v})_y = 0 \tag{37}$$

Under the boundary conditions (22), (30)–(32), Equation (29) can be averaged, yielding:

$$\begin{aligned}\epsilon^2 \mathrm{Pe}\left((h\langle uc\rangle)_x + (h\langle vc\rangle)_y\right) = \epsilon^2\left((h\langle c\rangle)_{xx} + (h\langle c\rangle)_{yy}\right) + \\ -\epsilon^2\left(c_x h_x + c h_{xx} + c_y h_y + c h_{yy}\right)|_h - \epsilon^2 \mathrm{Pe} q + \\ +\epsilon^4\left(h_x^2 + h_y^2\right)\left[\left(h_x c_x + h_y c_y\right)|_h - \mathrm{Pe} q\right]\end{aligned} \tag{38}$$

In order to arrive at the equation for the averaged quantities, the average velocity and concentration need to be separated from the components that depend on the z coordinate:

$$\boldsymbol{u}(x,y,z) = \bar{\boldsymbol{u}}(x,y) + \boldsymbol{u}'(x,y,z) \tag{39}$$

$$c(x,y,z) = \bar{c}(x,y) + c'(x,y,z) \tag{40}$$

where the average of the last term in both equations is equal to zero:

$$\int_0^h \boldsymbol{u}'(x,y,z)\,dz = \int_0^h c'(x,y,z)\,dz = 0 \tag{41}$$

It is assumed that:

$$c' \ll \bar{c} \tag{42}$$

This assumption is valid when transverse diffusion almost smoothed out the variation in the z-direction on the length scale L. In the mathematical sense, this can be written as:

$$L \gg \frac{H^2}{4D}\bar{u} \tag{43}$$

where $\frac{H^2}{4D}$ is the characteristic time after which the molecules travel from the middle of the channel to the wall. Using (4) and (16), this can be rewritten as:

$$\frac{1}{4}\epsilon^2 \mathrm{Pe} \ll 1 \tag{44}$$

As was shown before, the flow in the domain of interest can be classified as Hele-Shaw flow, thus the vertical distribution of the x and y components of the velocity is parabolic (26). Therefore, the changing part of the x and y components of the velocity can be approximated with the expression:

$$[u', v'] = -[\bar{u}, \bar{v}]\left(\frac{6z^2}{h^2} - \frac{6z}{h} + 1\right) \tag{45}$$

The equations include terms of different orders. From the assumption (44) and (4) one can find the following relations:

$$\epsilon^4 \ll \epsilon^4 \mathrm{Pe} \ll \epsilon^2 \ll \epsilon^2 \mathrm{Pe} \ll 1 \tag{46}$$

We will subsequently neglect terms of order smaller than ϵ^2.

By inserting the separated quantities into the averaged equation (38), the following equation is obtained:

$$\begin{aligned}\epsilon^2\mathrm{Pe}\left((h\bar{u}\bar{c})_x+(h\bar{v}\bar{c})_y+(h\langle u'c'\rangle)_x+(h\langle v'c'\rangle)_y\right)=\epsilon^2\left((h\bar{c})_{xx}+(h\bar{c})_{yy}\right)+\\ -\epsilon^2(\bar{c}h_x)_x-\epsilon^2(\bar{c}h_y)_y-\epsilon^2\left(c'_xh_x+c'h_{xx}+c'_yh_y+c'h_{yy}\right)\big|_h-\epsilon^2\mathrm{Pe}\,q\end{aligned} \tag{47}$$

Subsequently, the varying part of the concentration c' must be estimated in order to find the averages that depend on it ($\langle u'c'\rangle$ and $\langle v'c'\rangle$). To achieve this, the averaged equation (47) is subtracted from the main equation (15) and rewritten in terms of the separated variables (39)–(40).

The previous assumption on c' (42) allows us to introduce the varying part of the concentration in an expanded form:

$$c'=c'_0+\epsilon^2\mathrm{Pe}\,c'_1+\ldots \tag{48}$$

If the terms of order smaller than $\epsilon^2\mathrm{Pe}$ are neglected, the following is obtained after the averaged continuity equation (37) is invoked:

$$\begin{aligned}\epsilon^2\mathrm{Pe}\left(h\bar{u}c'_{0x}+hu'c'_{0x}-(h\langle u'c'_0\rangle)_x+h\bar{v}c'_{0y}+hv'c'_{0y}-(h\langle u'c'_0\rangle)_y+\bar{w}c'_{0z}+w'c'_{0z}\right)=\\ =-\epsilon^2\mathrm{Pe}(hu'\bar{c}_x+hv'\bar{c}_y)+hc'_{0zz}+\epsilon^2\mathrm{Pe}\,hc'_{1zz}+\epsilon^2\mathrm{Pe}\,q\end{aligned} \tag{49}$$

The first-order part of the above equation has the form $c'_{0zz}=0$, which can be easily solved using the conditions (30) and (41), to find:

$$c'_0=0 \tag{50}$$

The lower-order ($\epsilon^2\mathrm{Pe}$) of the expanded equation is:

$$c'_{1zz}=u'\bar{c}_x+v'\bar{c}_y-\frac{q}{h} \tag{51}$$

The lower-order equation is solved using estimation of u' and v' (45) and the conditions (30), (41), as previously, to find:

$$c'_1=-\left(\frac{z^4}{2h^2}-\frac{z^3}{h}+\frac{z^2}{2}-\frac{h^2}{60}\right)(\bar{u}\bar{c}_x+\bar{v}\bar{c}_y)+q\left(\frac{h}{6}-\frac{z^2}{2h}\right) \tag{52}$$

We then combine the formulas for u' and v' (45) with c' (48), (50), (52) to estimate the averages:

$$\langle u'c'\rangle=-\epsilon^2\mathrm{Pe}\left(\frac{\bar{c}_yh^2\bar{u}\bar{v}}{210}+\frac{\bar{c}_xh^2\bar{u}^2}{210}-\frac{hq\bar{u}}{60}\right) \tag{53}$$

$$\langle v'c'\rangle=-\epsilon^2\mathrm{Pe}\left(\frac{\bar{c}_xh^2\bar{u}\bar{v}}{210}+\frac{\bar{c}_yh^2\bar{v}^2}{210}-\frac{hq\bar{v}}{60}\right) \tag{54}$$

Finally, if the above averages along with the calculated estimates of c' (48), (50), (52) are inserted into (47), the final form of the averaged advection-diffusion equation is obtained:

$$\bar{J}^x_x+\bar{J}^y_y=S \tag{55}$$

where the averaged total fluxes $\bar{J}^x$, $\bar{J}^y$ and the source term S are defined as follows:

$$\bar{J}^x=h\bar{u}\bar{c}-\frac{1}{\mathrm{Pe}}h\bar{c}_x-\frac{\epsilon^2\mathrm{Pe}}{210}h^3\left(\bar{c}_y\bar{u}\bar{v}+\bar{c}_x\bar{u}^2\right) \tag{56}$$

$$\bar{J}^y = h\bar{v}\bar{c} - \frac{1}{\mathrm{Pe}} h\bar{c}_y - \frac{\epsilon^2 \mathrm{Pe}}{210} h^3 \left(\bar{c}_x \bar{u}\bar{v} + \bar{c}_y \bar{v}^2\right) \tag{57}$$

$$S = -\frac{\epsilon^2 \mathrm{Pe}}{60} \left[\left(h^2 q\bar{u}\right)_x + \left(h^2 q\bar{v}\right)_y\right] - q \tag{58}$$

Not only does the diffusive part of the equation include a correction due to the velocity, but also the source term includes terms of lower order. After these terms are neglected, the averaged advection-diffusion of the first order can be obtained as:

$$\left(h\bar{u}\bar{c} - \frac{1}{\mathrm{Pe}} h\bar{c}_x\right)_x + \left(h\bar{v}\bar{c} - \frac{1}{\mathrm{Pe}} h\bar{c}_y\right)_y = -q \tag{59}$$

The difference between the solutions of the two equations allows us to study the influence of the corrections on the main result. It is worth noticing that the first-order equation defined above no longer depends on ϵ. Clearly, ϵ influences only the corrections, therefore, as our results, we only present the distribution of the concentration for the general case (h, Pe).

3.3. Numerical scheme

To numerically solve the averaged advection-diffusion equation (55), the finite volume method was used, just as in case of the pressure equation (28). This time, however, the equation is similar to the equation of the two-dimensional stationary heat transfer in a non-homogeneous medium, but with the source term present [7].

To obtain a suitable numerical scheme, the averaged advection-diffusion equation (55) was integrated over the control volumes. In order to achieve this, the surface integrals over the CV (S) were transformed into integrals over its contour (∂S), using the 2D Gauss (divergence) theorem:

$$\int\int_S \nabla \bar{\boldsymbol{J}}\, ds = \int_{\partial S} \bar{\boldsymbol{J}} \boldsymbol{n}\, dl \tag{60}$$

for $\bar{\boldsymbol{J}} = (\bar{J}^x, \bar{J}^y)$, where $\boldsymbol{n}$ is the outward-pointing unit vector normal to the boundary of the CV at a given point, and ∇ is the 2D divergence operator. The left part of the equation was integrated over each boundary of the CV and the source term – over its volume. The distribution of the velocity, the height of the channel and the total fluxes over the boundaries of the CV were assumed to be constant, just as the distribution of the source term over the volume. Owing to this, the fluxes can be taken out of the integrals; also the terms with the $\bar{c}_y$ derivative in the $\bar{J}^x$ flux and the $\bar{c}_x$ derivative in the $\bar{J}^y$ flux (56)–(57) are lost. Nevertheless, these derivatives can be considered as terms of lower order, since they are taken in the directions parallel to the walls meaning they do not significantly affect the fluxes.

There are several ways to estimate the distribution of concentration between two nodes. In the *central scheme*, this distribution is assumed to be linear. For the

value on a boundary $i+\frac{1}{2}$ located between nodes (i,j) and $(i+1,j)$, this results in the following expressions for the concentration and its derivative:

$$\bar{c}_{i+\frac{1}{2}} = \frac{\bar{c}_{i+1,j}+\bar{c}_{i,j}}{2} \tag{61}$$

$$\bar{c}_{x;i+\frac{1}{2}} = \frac{\bar{c}_{i+1,j}-\bar{c}_{i,j}}{\Delta x} \tag{62}$$

where Δx is the distance between two nodes in the regular grid. Such scheme is not always valid, as it is expected that under the influence of a strong fluid flow, the value of the concentration on the boundary does not depend on the value at the node that lies downstream the flow. Therefore, in the *upwind scheme*, the value on the boundary is taken from the node situated upstream:

$$\bar{c}_{i+\frac{1}{2}} = \bar{c}_{i,j}, \quad \text{for } \bar{u}_{i+\frac{1}{2}} > 0 \tag{63}$$

$$\bar{c}_{i+\frac{1}{2}} = \bar{c}_{i-1,j}, \text{ for } \bar{u}_{i+\frac{1}{2}} < 0 \tag{64}$$

Since a constant value of the concentration in the area of the wall has been implicitly assumed, the derivatives are equal to zero. The transport of the analyte in the given direction is governed solely by advection.

Both schemes are valid only for certain values of the Peclet number, therefore the mixed *hybrid scheme* [8] is used, in which the central scheme is used for small values of the Peclet number while the upwind scheme is used for the large ones. Owing to this method, the coefficients of the numerical scheme will never be negative (which could explain the instability of the central scheme for the large values of the Peclet number). A detailed discussion of this problem is, however, beyond the scope of this work.

If the flow is assumed to satisfy the continuity equation (7) in the numerical sense, for each node (i,j) with the four neighbouring nodes $(i\pm1,j)$, $(i,j\pm1)$ and four boundaries of the CV $(i\pm\frac{1}{2})$, $(j\pm\frac{1}{2})$, the hybrid scheme yields an algebraic equation in the form:

$$a_{i,j}\bar{c}_{i,j} = a_{i-1,j}\bar{c}_{i-1,j} + a_{i+1,j}\bar{c}_{i+1,j} + a_{i,j+1}\bar{c}_{i,j+1} + a_{i,j-1}\bar{c}_{i,j-1} - s_{i,j} \tag{65}$$

where the coefficients are given by:

$$a_{i+1,j} = h_{i+\frac{1}{2}} \max\left[-\bar{u}_{i+\frac{1}{2}}, \frac{1}{\mathrm{Pe}\Delta x}\left(1+\frac{\epsilon^2\mathrm{Pe}^2 h^2_{i+\frac{1}{2}}\bar{u}^2_{i+\frac{1}{2}}}{210}\right) - \frac{\bar{u}_{i+\frac{1}{2}}}{2}, 0\right] \tag{66}$$

$$a_{i-1,j} = h_{i-\frac{1}{2}} \max\left[\bar{u}_{i-\frac{1}{2}}, \frac{1}{\mathrm{Pe}\Delta x}\left(1+\frac{\epsilon^2\mathrm{Pe}^2 h^2_{i-\frac{1}{2}}\bar{u}^2_{i-\frac{1}{2}}}{210}\right) + \frac{\bar{u}_{i-\frac{1}{2}}}{2}, 0\right] \tag{67}$$

$$a_{i,j+1} = h_{j+\frac{1}{2}} \max\left[-\bar{v}_{j+\frac{1}{2}}, \frac{1}{\mathrm{Pe}\Delta x}\left(1+\frac{\epsilon^2\mathrm{Pe}^2 h^2_{j+\frac{1}{2}}\bar{v}^2_{j+\frac{1}{2}}}{210}\right) - \frac{\bar{v}_{j+\frac{1}{2}}}{2}, 0\right] \tag{68}$$

$$a_{i,j-1} = h_{j-\frac{1}{2}} \max\left[\bar{v}_{j-\frac{1}{2}}, \frac{1}{\mathrm{Pe}\Delta x}\left(1+\frac{\epsilon^2\mathrm{Pe}^2 h^2_{j-\frac{1}{2}}\bar{v}^2_{j-\frac{1}{2}}}{210}\right) + \frac{\bar{v}_{j-\frac{1}{2}}}{2}, 0\right] \tag{69}$$

$$s_{i,j} = \frac{\epsilon^2 \mathrm{Pe}}{60}\left(h^2_{i+\frac{1}{2}} q_{i+\frac{1}{2}} \bar{u}_{i+\frac{1}{2}} - h^2_{i-\frac{1}{2}} q_{i-\frac{1}{2}} \bar{u}_{i-\frac{1}{2}}\right) + \\ + \frac{\epsilon^2 \mathrm{Pe}}{60}\left(h^2_{j+\frac{1}{2}} q_{j+\frac{1}{2}} \bar{u}_{j+\frac{1}{2}} - h^2_{j-\frac{1}{2}} q_{j-\frac{1}{2}} \bar{u}_{j-\frac{1}{2}}\right) + q_{i,j}\Delta x \tag{70}$$

$$a_{i,j} = a_{i+1,j} + a_{i-1,j} + a_{i,j+1} + a_{i,j-1} \tag{71}$$

This set of equations is solved using the ADI method, as in the case of the pressure equation. To obtain a numerical scheme for the simplified first-order averaged equation (59), it suffices to neglect the terms of order $\epsilon^2\mathrm{Pe}$ in the above formulae.

4. Validation

4.1. Parallel plates

To validate the numerical scheme for the transport equation, we simulated a simple case of a flat domain without any consumption of the analyte. In such a case, we have $c = c(x,y,z)$, $u = u(x,z)$, $v(x,y,z) = 0$, $w(x,y,z) = 0$, $q = 0$ and $h = \mathrm{const}$. These variables are inserted into the averaged advection-diffusion equation (55) to obtain:

$$(\bar{u}\bar{c})_x - \frac{\epsilon^2 \mathrm{Pe}}{210}\left(\bar{c}_x \bar{u}^2\right)_x - \frac{1}{\mathrm{Pe}}(\bar{c}_{xx} + \bar{c}_{yy}) = 0 \tag{72}$$

The obtained results were compared with the result of the experiment performed by Kraus *et al.* [9], in which a dye with a diffusion coefficient of $D = 5.68 \cdot 10^{-10}$ m^2/s was added to the flow in a square reaction chamber of 1 cm $\times$ 1 cm and investigated through the light transmission measurement. The height of the channel was $H = 525$ μm and the overall flow rate was equal to 61 μL/min, which corresponds to an average flow velocity of $u_0 = 1.936 \cdot 10^{-4}$ m/s. The flow is laminar, as the Reynolds number is $\mathrm{Re} = \frac{u_0 H}{\nu} \approx 0.14$. The inlet of the dye is said to be located in the centre of the channel. The average flow velocity is assumed to approximate the velocity in the centre of the channel averaged over the z-direction, therefore the channel can be approximated by the infinite parallel plate model, neglecting the influence of the vertical side walls. Bruus [10] discovered that the difference in flux between the exact and approximated solution is of the order of 23% for an aspect ratio between the height and width of the channel of 1/3, and 7% for 0.1. Assuming the error varies linearly with the aspect ratio, the error caused by the presence of side walls is expected to be around 3% in the present case, where $H/B = 0.0525$, which we believe to be acceptable for the current purpose.

Because of the lack of the cell spot, the length of the computational domain $L = 1$ cm was chosen for the spatial scale for the model, yielding an aspect ratio of $\epsilon = 0.0525$ and the value of the Peclet number for the whole domain of $\mathrm{Pe} = 3408$. These values are somewhat outside the domain of usability of the present model, yielding $\epsilon^2\mathrm{Pe} \approx 9.4$, compared to (44). Nevertheless, the results are expected to qualitatively agree with experiment.

According to the well-known model of light absorption in soluble matter, the change of light intensity $dI(x,y)$ due to absorption by an infinitesimal layer of fluid dz is $dI = -\alpha c I\, dz$. The equation can be solved to obtain the formula for the light intensity as a function of the concentration of the nutrient:

$$I(c) = e^{-\alpha c} \tag{73}$$

The normalisation parameter α was chosen so as to reflect given results [9].

Figure 4 presents both the measured and calculated absorption profile obtained by Kraus *et al.* [9]. The graphs show the light intensity profiles for ten crossections of the channel, equally spaced along the x-axis. The employed computational model was based on the analytical solution for a point source. Kraus *et al.* [9] conclude that an overall broadening very similar to the one measured was observed, although the unexpectedly high absorption profile at the centre of the stream was not reflected by the computational model. This is believed to be due to local 3D effects near the injection geometry and due to velocity gradients in the (x,z)-plane, which were not taken into account in the simulation. The model employed was not able to make use of the exact absorption profile measured at the inlet, therefore a step function was used.

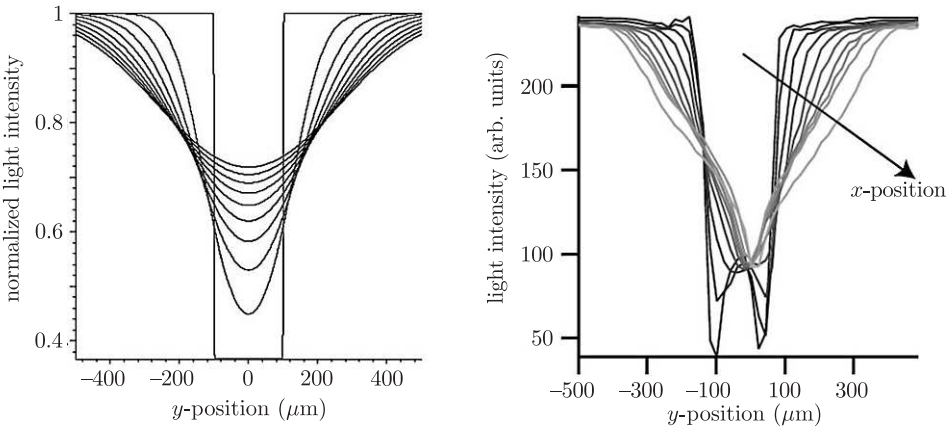

Figure 4. Results obtained by Kraus *et al.* [9]. The left panel presents the calculations performed by Kraus *et al.* using the model based on the superposition of analytical solutions for point sources; the right panel presents the results of the experiment. The narrowest line corresponds to the absorption profile measured at the inlet. The other profiles were measured with 1 mm increments in the x-position

Figure 5 presents the results obtained using the proposed model. Calculations were performed for two cases of the boundary conditions at the inlet – a step function and the exact distribution obtained from the experiment using Equation (73). The results for a step function are very similar to the numerical results obtained by Kraus *et al.* Unfortunately, incorporating the exact conditions at the inlet did not significantly affect the results. As the current model takes the velocity gradients in the (x,z)-plane into account as a Taylor dispersion correction

(Figure 6), the additional variations in the concentration that were measured are believed to be due to other 3D effects. The Taylor dispersion correction obtained for the given case is of significant order, however, the set of parameters (Pe, ϵ) for the given problem was slightly outside the assumed range of the values allowed for the model.

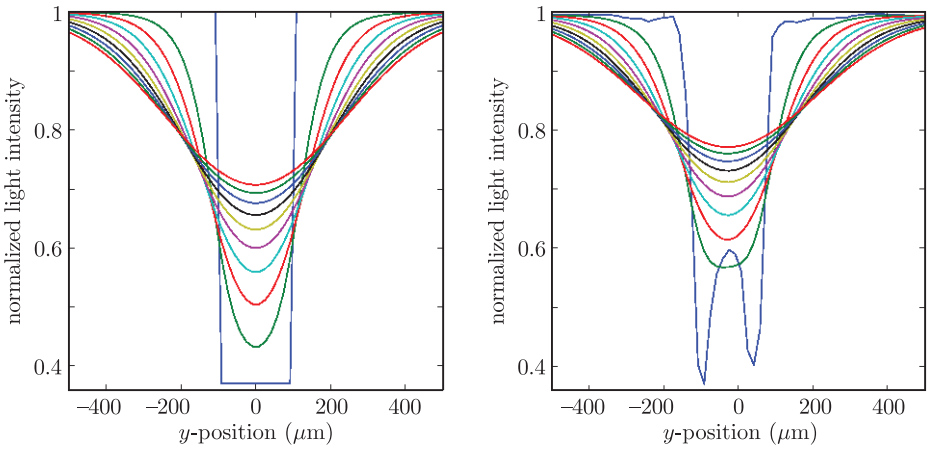

Figure 5. Results obtained with the current method. The left panel corresponds to the simplified distribution at the inlet, the right panel corresponds to exact inlet conditions taken from the experimental results (Figure 4)

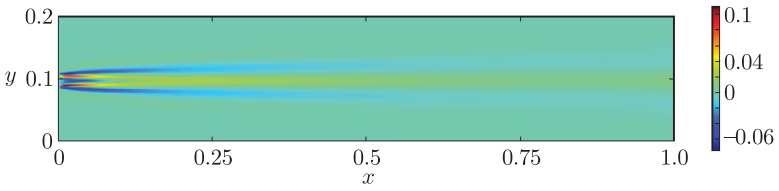

Figure 6. Influence of the Taylor dispersion correction across the channel, computed with the current method for the case described in [9]. The plot presents the difference between normalized light intensities calculated with and without the Taylor dispersion correction

4.2. Flow around a cell spot

A qualitative test for the validity of numerical calculations of the laminar flow around a cell spot was proposed by Walker *et al.* [11], who suggest that the treatment of the cell spot with two laminar fluid streams requires the interface between the streams to be positioned exactly in the middle of the spot. Otherwise, the laminar flow would cause the spot to be exposed to the contents of only one stream. Such a numerical experiment was performed using the proposed method. To represent a round spot with a unit radius, a particular function was chosen:

$$h(r) = \begin{cases} 1 - \frac{1+cos(r^2\pi)}{2} h_f & \text{if } r \leq 1 \\ 1 & \text{if } r > 1 \end{cases} \tag{74}$$

where r is the distance from the centre of the spot, and the parameter h_f is the fraction of the height of the channel occupied by the cell spot in its centre. A particular case, where the computational domain is a rectangle 5×12, with the spot located at (2.5,3) is shown in Figure 7. The size of computational area and the location of the cell spot, together with the parameters r and h, are given in the dimensionless form (5)–(6). The velocity field obtained for $h_f = 0.5$ is presented in Figure 8. The concentration distribution at the inlet was given in the form of a step function, resembling the case with two streams, one of which carries the analyte. The interface between the streams was set slightly off the centre of the spot.

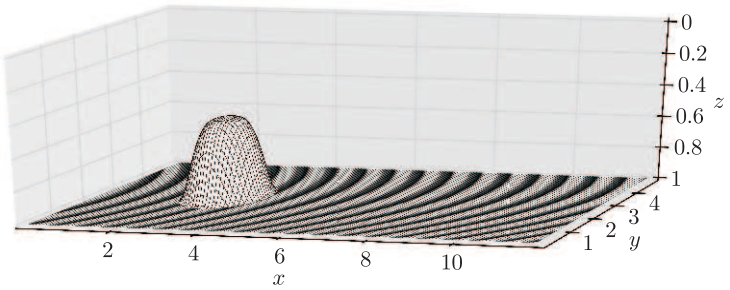

Figure 7. Graph of a particular cell spot for the case $h_f = 0.5$

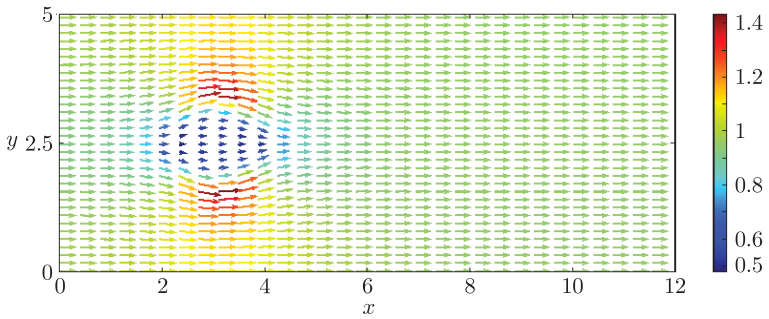

Figure 8. Velocity field around the spot; $h_f = 0.5$; the colour indicates the magnitude of the velocity vector

The numerical calculations for the concentration distribution were performed for $\mathrm{Pe} = 2000$, $\epsilon = 0.02$. The results (Figure 9) clearly reflect the behaviour described in [11]. The interface between the two streams is effectively pushed away from the spot. This can be clearly seen by comparing with the case without the influence of the presence of the spot (Figure 10). The analyte from the carrying stream is transported to the second stream by means of diffusion. This process is also influenced by the flow profile.

4.3. Stability of the flux throughout the domain

One of the most basic and important requirements for a numerical application is the lack of numerical divergence. The finite volume method that was

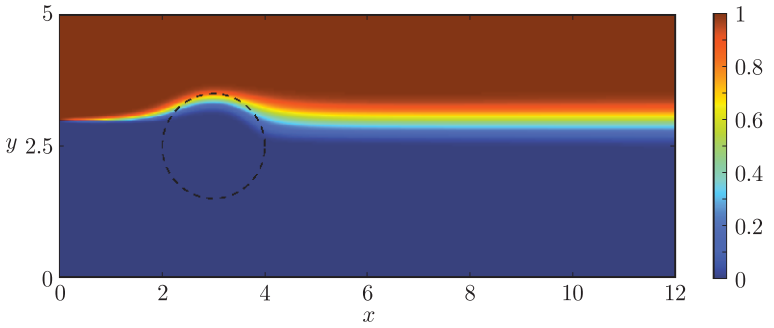

Figure 9. Distribution of concentration influenced by the velocity field due to the presence of the cell spot; the position of the spot is indicated with the dashed line

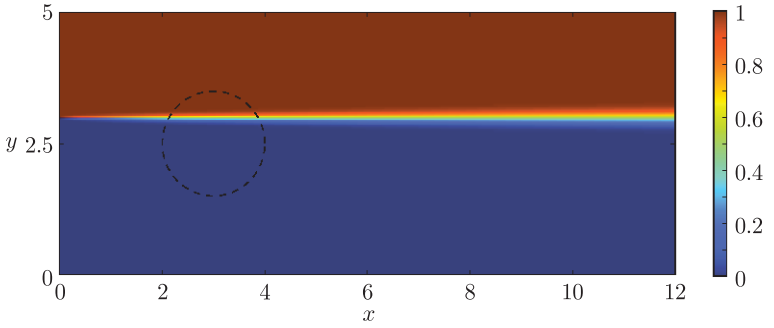

Figure 10. Distribution of concentration without taking into account the presence of the cell spot

used here naturally incorporates this feature, as it is based on the calculation of fluxes over the boundaries of computational cells. The total flux of concentration through the channel is calculated by integrating the flux J^x (56) over the entire cross-section of the channel for different x-positions.

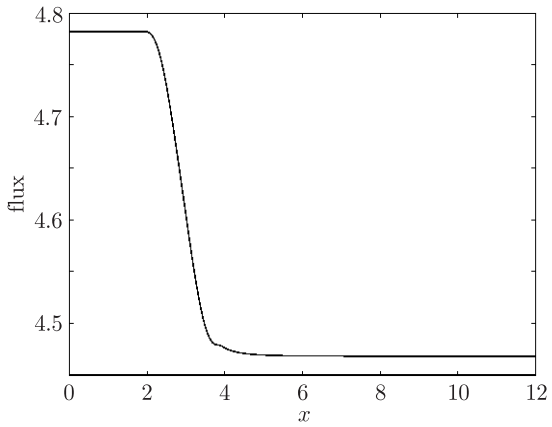

Figure 11. Flux of concentration throughout the channel. A spot of radius $R_S = 1$ and height $h_f = 0.5$ is located at $x = 3$

From the plot of the flux of concentration for different cross-sections of the channel (Figure 11), we can see that the numerical code is well-behaved: the flux is constant, and the only changes are due to the absorption of the nutrient in the area of the spot. There are no artificial sources or sinks in the computational area.

5. Numerical results of concentration distribution

To represent the intensity of consumption of the nutrient across the channel and across the spot itself, we must choose a suitable function $q(x,y)$. A detailed discussion of this topic is beyond the scope of this work, but we can assume that the intensity depends on the distance from the centre of the spot, in the similar way as the height of the spot does. For simplicity, we assume a function analogous to $h(x,y)$:

$$q(r) = \begin{cases} \frac{1+cos(r^2\pi)}{2} Q & \text{if } r \leq 1 \\ 0 & \text{if } r > 1 \end{cases} \tag{75}$$

Different values of Q result in different uptakes. The depletion of the concentration is different for different heights, as it depends on the thickness of the fluid above the spot. To allow comparison of results, the value of Q was kept constant (0.2) and two cases were studied: $h_f = 0.0$ (no influence of the spot on the flow) and $h_f = 0.5$. This results in different minimum values of the concentration for the two cases (Figures 12 and 13), while the uptake is believed to be of the same order.

The graphs for the case of $h_f = 0.5$ (Figures 13 and 14) show the contraction of the wake due to the specific velocity distribution at the rear of the spot (Figure 8). This effect becomes stronger as the Peclet number grows. No such effect was observed in the case of parallel plates, where the width of the wake is similar to the diameter of the spot. This phenomenon is deemed interesting and requires further study.

The theoretical analysis of averaged advection-diffusion equations (56)–(57) shows that the effect of Taylor dispersion is significant only in the area where the fluid flows in the direction parallel to the concentration gradient. In our case, this took place in the area of the spot (Figure 15). Still, for the considered values of ϵ and Pe, the corrections of order ϵ^2Pe are negligible when compared to the order of the main result (compare Figures 13 and 15). This indicates that the effect of Taylor dispersion does not play an essential role in our model. One of the reasons for this is the assumption $\epsilon^2 \mathrm{Pe} \ll 1$ (46), which does not allow us to select all possible values of Pe and ϵ from the ranges defined in Table 1.

According to Table 1, a typical distance between two successive spots in the device is an order of magnitude larger the diameter of the spot. This corresponds to our computational area, in which the next spot may be located just beside the outlet. Because of the high concentration of the wake for $\mathrm{Pe} = 300$ (Figures 12–13), it is not reasonable to assume that the successive spots do not affect one another. Decreasing the Peclet number by one order of magnitude (to $\mathrm{Pe} = 30$) resulted in a significant smoothing out of the wake by diffusion before it reached the outlet (Figure 14).

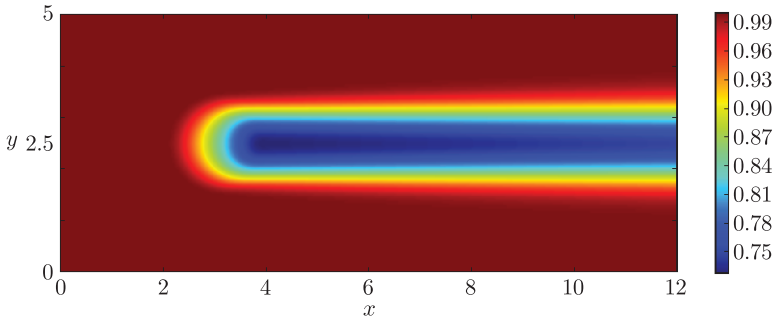

Figure 12. Concentration of the nutrient, $h_f = 0.0$, $\mathrm{Pe} = 300$

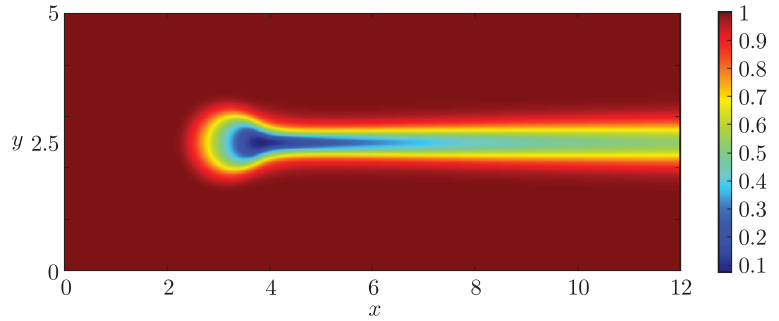

Figure 13. Concentration of the nutrient, $h_f = 0.5$, $\mathrm{Pe} = 300$

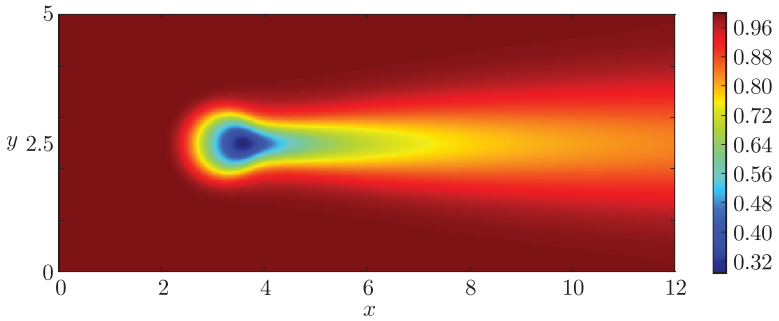

Figure 14. Concentration of the nutrient, $h_f = 0.5$, $\mathrm{Pe} = 30$

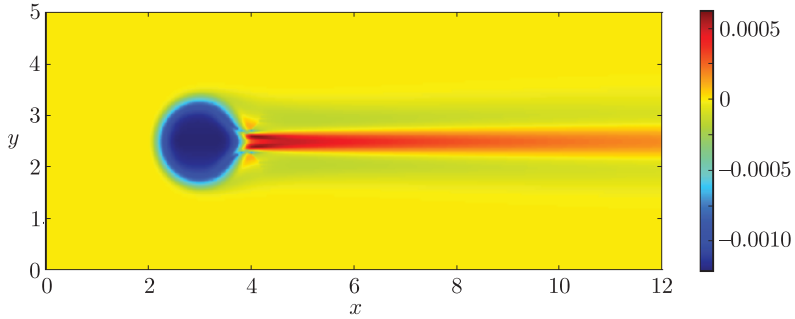

Figure 15. Influence of the correction terms: $h_f = 0.5$, $\mathrm{Pe} = 300$, $\epsilon = 0.05$

6. Conclusions

In this work, we developed a numerical model for the fluid flow and cell nutrient concentration in a micro-fluidic device. In particular, we considered the region where cells are cultured. This area is typically a very shallow environment where the fluid carrying the cell nutrient flows slowly. As the fluid passes over the cell spot, the nutrient concentration decreases and, behind the cell spot, a wake of a depleted nutrient is generated. Concentration gradients in the wake are then smoothed out by diffusion and advection. The ability to predict the concentration values behind each cell spot and the evolution of the wake are of fundamental importance for the proper use of the microdevice. Indeed, cell spots may be placed in various locations across the channel, and the concentration in a cell spot may be influenced by the depletion of nutrient induced by cells located upstream.

This work was aimed at investigating the above phenomeonn, taking into account the influence of the presence of the cell spot on the size of the wake and the concentration within it. Modelling of fluid flow and the evolution of concentration were performed with a two-dimensional model. Owing to the fact that the domain is very shallow, fluid flow is governed by a linear equation for the pressure (Hele-Show flow). The laminar flow around the cell spot highly influences the shape and intensity of the depleted wake, resulting in narrowing downstream.

For the advection-diffusion equation, the effect of Taylor dispersion was taken into account by the application of an asymptotic expansion. The small parameter is $\epsilon^2\mathrm{Pe}$, where ϵ is the ratio of the thickness of the domain to the diameter of the cell spot, and Pe is the Peclet number of the flow. It was shown that the corrections to the leading-order equation due to Taylor dispersion come into play at the order $\epsilon^2\mathrm{Pe}$ and thus are, in general, insignificant. On the other hand, Taylor dispersion was found to be of crucial importance for the unsteady cases and, therefore, an extension of the current model to non-stationary problems would be desirable and would enable a detailed study of this effect.

In this work, the flux of nutrient consumption (described by the uptake function) was arbitrarily chosen as proportional to the height of the cell spot. Although such a function enables the study of particular cases, refinements to this approach are suggested for the model to be more realistic and flexible. In particular, it would be very interesting to couple the nutrient uptake with the concentration and cell state. This could be performed, for instance, using the Michaelis-Menten model. Also, this might enable predicting the ideal thickness of the domain, which would then allow sufficient cell nutrition with maximum possible reduction in the magnitude of the wake behind each cell spot.

The problems of fluid dynamics involving the combined effects of convection and diffusion are not easy to solve and usually require special treatment for each particular case. Careful validation of the code is always required, and therefore it was one of the major aims of this work. Two simplified cases, both without the consumption of the nutrient were considered – a case of parallel plates and

of a round cell spot with an off-centre step in concentration. Comparison with available literature data proved that the model gives satisfactory results under a wide range of conditions.

Acknowledgements

This work is based on the author's Master's Thesis entitled *Two-dimensional model of fluid flow and distribution of nutrient concentration in a microfluidic device*. The thesis was written under the supervision of prof. Rodolfo Repetto from the University of Genoa as part of the double diploma programme between Gdansk University of Technology and the University of L'Aquila.

References

[1] Chung B G, Flanagan L A, Rhee S W, Schwartz P H, Lee A P, Monuki E S and Jeon N L 2005 *Lab on a Chip* **5** (4) 401
[2] Kim L, Toh Y C, Voldman J and Yu H 2007 *Lab on a Chip* **7** 681
[3] Reyes D R, D. Iossifidis, Auroux P A and Manz A 2002 *Analytical Chemistry* **74** (12) 2623
[4] Auroux P A, Iossifidis D, Reyes D R and Manz A 2002 *Analytical Chemistry* **74** (12) 2636
[5] Repetto R, Malvin T, Brooks S, Jones M, Friedrich D, King J, Waters S, Gratton M, Oliver J and Witelski T 2007 *Bio-opto-micro-fluidic Devices for Cell Interrogations*, 7$^{\text{th}}$ Mathematics in Medicine Study Group, University of Southampton
[6] Taylor G 1957 *Dispersion of Soluble Matter in Solvent Flowing Slowly through a Tube*, Proc. Royal Society of London, Series A, Mathematical and Physical Sciences
[7] Minkowycz W J, Sparrow E M, Schneider G E and Pletcher R H 1988 *Handbook of Numerical Heat Transfer*, Wiley
[8] Mikielewicz D 2007 *Computer Methods in Heat Transfer*, Lecture Notes, Gdansk University of Technology (in Polish)
[9] Kraus T, Verpoorte E, Linder V, Franks W, Hierlemann A, Heer F, Hafizovic S, Fujii T, Rooija N F de and Koster S 2006 *Lab on a Chip* **6** 218
[10] Bruus H 2008 *Theoretical Microfluidics*, Oxford University Press
[11] Walker G M, Zeringueb H C and Beebe D J 2004 *Lab on a Chip* **4** 91